Systematic study of electron localization in an amorphous semiconductor

Raymond Atta-Fynn,[1] Parthapratim Biswas,[1] Pablo Ordejón,[1,2] and D. A. Drabold[1,*]
[1]*Department of Physics and Astronomy, Ohio University, Athens, Ohio 45701-2979, USA*
[2]*Institut de Ciència de Materials de Barcelona (CSIC), Campus UAB, 08193 Bellaterra, Spain*
(Received 10 October 2003; published 26 February 2004)

We investigate the electronic structure of gap and band tail states in amorphous silicon. Starting with two 216-atom models of amorphous silicon with defect concentration close to the experiments, we systematically study the dependence of electron localization on basis set, density functional, and spin polarization using the first-principles density-functional code SIESTA. We briefly compare three different schemes for characterizing localization: information entropy, inverse participation ratio, and spatial variance. Our results show that to accurately describe defected structures within self-consistent density-functional theory, a rich basis set is necessary. Our study revealed that the localization of the wave function associated with the defect states decreases with larger basis sets and there is some enhancement of localization from generalized gradient approximation relative to local-density approximation. Spin localization results obtained via local spin-density approximation (LSDA) calculations are in reasonable agreement with experiment and with previous LSDA calculations on *a*-Si:H models.

DOI: 10.1103/PhysRevB.69.085207 PACS number(s): 71.23.Cq, 71.15.Mb, 71.23.An

I. INTRODUCTION

Amorphous semiconductors represent a large and important area in materials science, with interest both from the technological and fundamental point of view. Coordination defects in *a*-Si are of key importance to bulk and transport properties. Understanding the nature of defects in *a*-Si can help unlock the mystery behind phenomena such as the Staebler-Wronski effect[1] and help establish the link between localization of defect states and large electron-phonon coupling. Early theoretical work on defect states in *a*-Si and *a*-Si:H was based on tight-binding methods.[2–7] For example, Biswas *et al*.[2] and Fedders and Carlsson[4] investigated the electronic structure of dangling and floating bonds in *a*-Si. They showed that gap defect states associated with dangling bonds are strongly localized on the central atom of the dangling bond.[2] More recently, density-functional calculations of dangling-bond states using the local-density approximation[8] (LDA) have been performed by Fedders and Drabold.[9] They reported a wave-function localization of 10–15 % on the central atom in supercell models with one defect and far less on supercell models with many defects due to defect band formation. This finding was at variance with electron-spin resonance (ESR) experiments, which showed that over 50% of spin density of the gap state is located on the central atom of the dangling bond.[10,11] However, recent calculations by Fedders *et al*.,[12] using the local spin-density approximation (LSDA), have shown that a large spin localization of a defect state does not necessarily imply the existence of a corresponding wave-function localization.

Density-functional theory[13] (DFT) has enjoyed enormous success in describing the ground-state properties and defects for a wide range of materials, and in particular, *a*-Si. Nonetheless, the one-particle Kohn-Sham energies in the theory have no formal justification as quasiparticle energies. However from an empirical point of view, Hybertsen and Louie have shown, using GW calculations,[14] that for states close to the fundamental band edges of bulk semiconductors and in particular Si, there is a 99.9% overlap of the quasiparticle wave function with the corresponding Kohn-Sham orbital (GW calculations provide post Hartree self-energy corrections to DFT/LDA). This provides some rationale for interpreting the Kohn-Sham orbitals as quasiparticle states.

Within the density-functional framework, there is a general problem for the accurate representation of localized midgap and band tail states in amorphous semiconductors. The reliability of density-functionals to correctly reveal the localized behavior of electronic states with respect to its wave function and spin is very important. In particular, the generalized gradient approximation (GGA) and LSDA results for electron localization are sometimes quite different. For example, recent density functional and GW studies of the metal-insulator transition of bcc hydrogen showed that eigenfunctions obtained GGA are more localized[15,16] and closer to quasiparticle energies and states than LSDA. Also, it was observed that GGA band gap was systematically larger than LSDA gap.[15]

In this paper, we systematically examine the localization of band tail and gap states and its dependence on basis sets, density functionals, and spin polarization for three defected models: two 216-atom supercell models of amorphous Si and a 218-atom supercell model of crystalline Si:H with a vacancy. The crystalline model will serve as a benchmark to compare the nature of a dangling-bond defect state in an amorphous environment with that of the crystalline phase. We compare the localization of gap and tail states within the LDA, LSDA, and GGA for frozen lattices (unrelaxed samples) as well as for samples fully relaxed for a given Hamiltonian. Our motivation for performing the frozen lattice calculation is to systematically investigate the sole effect of different basis sets and density functionals on the localization of states for a fixed configuration. We study the relaxation effects to see the dependence of the local geometry of the defect sites on the different basis orbitals and density functionals and the behavior of localized defect states in a relaxed environment compared to the frozen one. We com-

puted spin and wave-function localization for defect states, to determine the correlation between spin density and charge density.

II. METHODOLOGY

A. Models and calculations

Two of the models used here were generated by Barkema and Mousseau[17] using an improved version of the Wooten, Winer, and Weaire (WWW) algorithm.[18] The details of the construction was reported in Ref. 19 and we just give a brief recap here. Two independent 216-atom models of *a*-Si, each with two dangling bonds, were generated. Atoms are first packed randomly in a box, at crystalline density, with the single constraint that no two atoms be closer than 2.3 Å. A connectivity table was then set up by constructing a loop that passes exactly twice through each atom. To create a dangling bond, a ghost bond (bond with zero energy) is placed between two atoms. The two atoms are chosen in such a way that they are quite close in one model and reasonably far in another model. The network is then relaxed using a fixed list of neighbors and a Keating potential. These steps ensure that the initial state has no trace of crystallinity. The models are then relaxed using a series of WWW moves, using the accelerated algorithm discussed in Ref. 5. The conformations are finally relaxed at zero pressure with a Keating potential. In this work we refer these two 216-atom supercell models of *a*-Si as CLOSE and FAR. In model CLOSE the atoms with the dangling bonds are separated by a distance of 4.6 Å, whereas in the model FAR they are 7.7 Å apart. The third model, which we will refer to as *c*-Si:H, is generated as follows: starting with a 216-atom cell of silicon in the diamond structure, an atom is removed resulting in the creation of a vacancy with four dangling bonds. Three of them were terminated by placing a H atom at about 1.5 Å from the corresponding threefold-coordinated Si atom. This results in one isolated dangling bond. Throughout this work, we will use a cutoff radius $R_{\text{Si-Si}}=2.6$ Å to define Si-Si coordination.

Our DFT calculations were performed within the LDA (with and without spin polarization) and the GGA using the code SIESTA.[19–21] We used the parametrization of Perdew and Zunger[22] for the exchange-correlation functional in all LDA calculations and that of Perdew, Burke, and Ernzerhof[23] for the exchange-correlation functional in all GGA calculations. Norm conserving Troullier-Martins pseudopotentials[24] factorized in the Kleinman-Bylander form[25] were used to remove core electrons. To describe the valence electrons, we used atomic orbitals basis set consisting of finite-range numerical pseudoatomic wave functions of the form proposed by Sankey and Niklewski.[26] We employ single ζ (SZ) and double ζ with polarization functions (DZP) basis sets on all the atoms.[27] We solved the self-consistent Kohn-Sham equations by direct diagonalization of the Hamiltonian. The Γ point was used to sample the Brillouin zone in all calculations.

B. Quantifying the degree of localization

To characterize the spatial extent of an electronic state we use three measures of localization. Two of them depend on the Mulliken (point) charge[28] $q_i(E)$ residing at an atomic site i for an eigenstate with energy eigenvalue E. The charges are normalized $[\Sigma_{i=1}^{N} q_i(E)=1$, where N is the total number of atoms in the supercell]. The third is a measure of the spread of the wave function in real space, as the second moment of the radial displacement about its center (variance). We briefly describe below each measure and its interpretation.

The first quantity, the conventional inverse participation ratio (IPR)

$$I(E)=\sum_{i=1}^{N} [q_i(E)]^2, \tag{1}$$

is a measure of the inverse of the number of sites involved in the state with energy E. For a uniformly extended state, the Mulliken charge contribution per site is uniform and equals $1/N$ and so $I(E)=1/N$. For an ideally localized state, only one atomic site contributes all the charge and so $I(E)=1$. This implies that high values of $I(E)$ correspond to localized states and low values correspond to delocalized states. Despite its ubiquity, the IPR is an *ad hoc* measure of localization. The second quantity has been used by Lewis *et al.*[29,30] to measure the localization of DNA electron states. It utilizes the information entropy[31,32] $S(E)$ of an eigenstate with energy E and is given by

$$W(E)=\exp[S(E)], \tag{2}$$

where $S(E)=-\Sigma_{i=1}^{N} q_i(E) ln\, q_i(E)$. In information theory, the entropy is a measure of disorder or randomness in the $\{q_i\}$. As such, it has more *a priori* justification for use as a measure of localization. This is especially true if we interpret localization as a *departure from randomness*.[33] We interpret $W(E)$ as an estimate of the *number of accessible atoms* for a given state or equivalently, the number of atoms a particular electronic state can reach. It follows that $W(E)$ ranges from the total number of atoms for a uniformly extended state (that is, all the atoms are accessible) to unity for an ideally localized state (that is, only one atom is accessible). For purposes of discussions and comparisons to IPR, we use $1/W(E)$ for our work.

The third quantity we use to determine the localization of the wave functions is a measure of the spread in real space, as defined in the context of localized wave functions in molecules[34] and maximally localized Wannier functions in solids.[35,36] This definition assumes that the wave function has a well-defined center, and that the average of the position operator can be defined. This is not the case for our eigenstates, which correspond to the Γ point and therefore are periodic in the supercell. However, since we are interested in states which are localized (exponentially) within the supercell, we can still use the definition of the spread, by integrating over the cubic supercell volume centered at the defect site:

$$\sigma^2=[\langle \mathbf{r}^2\rangle-\langle \mathbf{r}\rangle^2]. \tag{3}$$

We also compute the amount of the norm of the wave function that is around the defect center, by integrating over a sphere Ω centered at the defect and which has the same

diameter as the lattice constant (so it is the largest sphere that fits into the supercell volume). Clearly, the defect states will not be completely localized within the sphere, and the norm of the wave function inside the integration volume, q_Ω, will be smaller than 1. This is also a measure of the amount of wave function which is outside the integration sphere: for an extended state, the amount of charge will be close to one-half, since the sphere encloses approximately half the supercell volume. For localized states, we typically capture more than 80% of the wave-function norm. We will characterize the localization by using both the spread σ^2 (larger values correspond to less localization) and by the norm q_Ω.

III. RESULTS

A. Frozen lattice calculations

1. Wave-function localization

In order to understand the effect of basis set and density functional on the localization of defects states, we first compute the electronic structure of the three models with fixed geometry, using the different basis sets and density functionals.[37] We begin our discussion with simplest of the three models, *c*-Si:H. The position and localization for individual states are reported in Figs. 1 and 2, where the IPR and $1/W(E)$, respectively, are used to measure localization. Each spike indicates an energy eigenvalue. With both measures of localization, and for all basis sets and density functionals considered, we observe a highly localized state near at Fermi level, with all the other states being extended. This state is centered on the dangling-bond atom, which contributes with a Mulliken charge of $0.54e$ and $0.57e$ in the SZ-LDA and SZ-GGA cases, respectively, and $0.27e$ and $0.31e$ in the DZP-LDA and DZP-GGA cases, respectively. The rest of the state is mainly localized in the neighbor atoms to the dangling bond. Both the IPR and $1/W(E)$ provide the same qualitative picture of the localized state, and its evolution with basis set and density functional. In particular, localization decreases strongly when we go from the SZ basis to a more complete DZP basis. It also increases but only by a small amount when using GGA instead of LDA. These are general trends which we will also observe with the other models, as we will see below. We note that the decrease in the measure of localization is not proportional to the decrease in the Mulliken charges at the defect state, as both definitions of localization are nonlinear. While the charge at the dangling-bond site is reduced by a factor of 2 when moving from SZ to DZP, the localization measure decreases by roughly a factor of 3, both for IPR and $1/W(E)$.

Unlike $I(E)$ and $W(E)$ that are point estimators of the localization (in the sense that they use only the Mulliken charge at each atomic site), σ^2 is a more physical representation. The results obtained for σ^2 for *c*-Si:H with the lattice frozen are presented in Table I. The spread for the localized state *M* is simple to compute since it is unimodal (peaked at only one site and therefore having a well-defined center). From σ^2, we also see monotonic increase in the spread and a decrease in the total charge in the localization volume as the basis sets are increased (see Table I). The GGA states show a slightly smaller spread than the corresponding LDA states. In Fig. 3 we show snapshots of the isosurface of the wave function for the localized midgap state of *c*-Si:H within two approximations. We see a dangling-bond orbital confined to a small region in space in the SZ case implying that the state is well localized. In the DZP case, we see pieces of the surface in the vacancy and other neighboring atoms besides the dangling-bond orbital making it less localized compared to the SZ case.

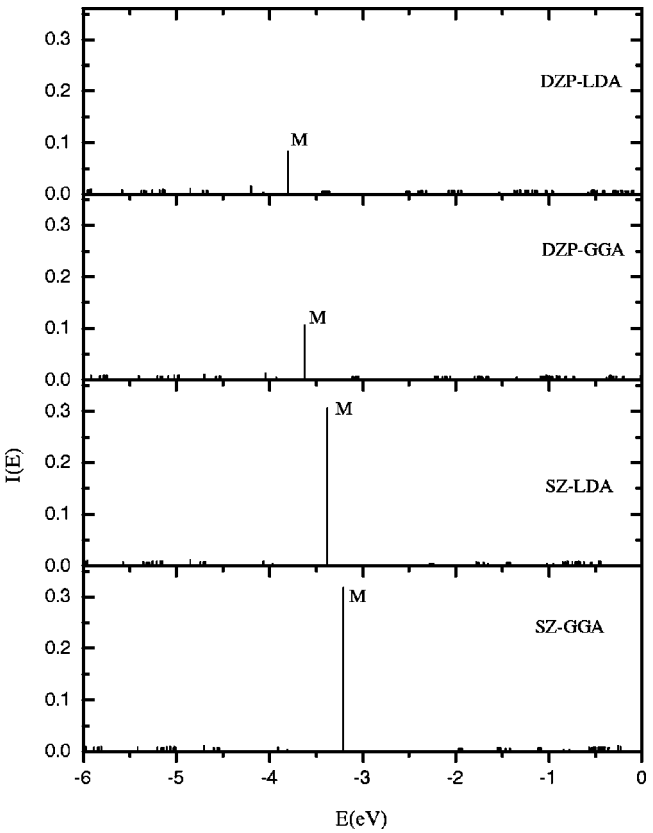

FIG. 1. IPR for the model *c*-Si:H computed using frozen coordinates. The highly localized midgap state (labeled *M*) sits on the central atom of the dangling bond. For the SZ basis functions the charge localization on the central atom within the LDA and GGA are, respectively, $0.54e$ and $0.57e$. For the DZP basis sets, the charge localization on the atom reduces to $0.27e$ and $0.31e$, respectively, within the LDA and GGA.

Next, we analyze the localized nature of the states for the amorphous model CLOSE. In this system, we expect to see two localized states in the gap, corresponding to the two dangling bonds present in the structure. Indeed, we see two highly localized gap states *H* and *L* in the IPR shown in Fig. 4, with an energy splitting which is just over a tenth of an eV. The state *H* is the highest occupied molecular orbital (HOMO) and *L* is the lowest unoccupied molecular orbital (LUMO). Due to the small distance between the two dangling bonds, the localized *H* and *L* states are bonding and antibonding combinations of the dangling-bond states, and therefore both *H* and *L* have nearly equal weights on the two defect sites. In the SZ case, the total Mulliken charge contributions from the two dangling-bond sites for each of the two localized wave functions range between $0.52e$ and $0.64e$.

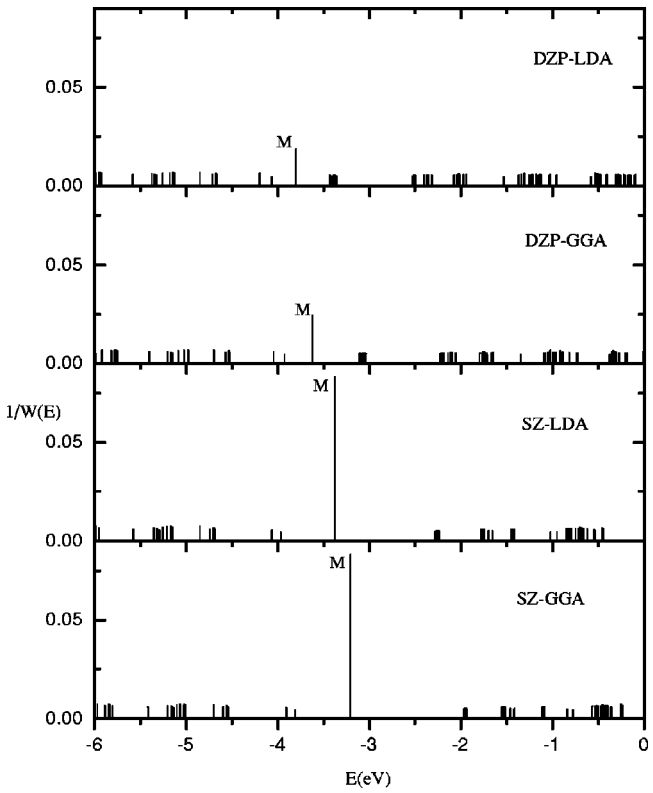

FIG. 2. Localization of states [as measured using $1/W(E)$] for the model c-Si:H using the frozen lattice. The only localized midgap state (labeled M) sits on the central atom of the dangling bond.

The charge concentrations drop to the range $0.29e$-$0.40e$ in the DZP case. In Fig. 5, we show the results for $1/W(E)$. We see a sharp drop in the number of atoms a given eigenstate can reach as the energy changes from the edge of either the valence or conduction band into the gap. We again see that all the features of $I(E)$ are reproduced in $1/W(E)$. For each localized state, both measures decrease by approximately a factor of 2 when the basis sets are increased from SZ to DZP.

In Fig. 6, we show the IPR for the model FAR. As in the CLOSE case, both the HOMO and LUMO states are localized. Now, however, since the distance between the two dangling-bond sites is larger, the HOMO-LUMO splitting is much smaller, only ~ 6 meV. The HOMO has now most of its weight on one of the dangling bonds, whereas the LUMO is mostly localized in the other. The trend in localization of the gap states is similar to the trend observed in the other two models, decreasing strongly with more complete basis sets.

TABLE I. The frozen lattice results for the spread σ^2 and the charge integrated over a sphere q_Ω for the localized midgap state M for the supercell c-Si:H. Unit for σ^2 is Å^2.

Functional	Basis	σ^2	q_Ω
LDA	DZP	32.14	0.80
GGA	DZP	28.46	0.83
LDA	SZ	19.44	0.90
GGA	SZ	18.55	0.91

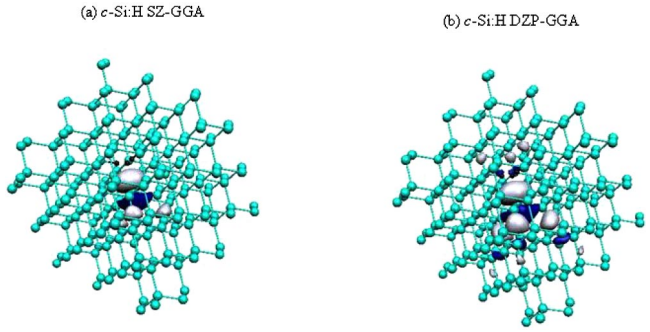

FIG. 3. (Color online) Isosurface plots for localized wave functions corresponding to a c-Si:H dangling-bond defect state. The wave functions were generated with the same cutoff. Each surface is labeled according to the basis set and functional used. The surface is confined to a small region in space in the simple SZ case. For the DZP basis we see a localized dangling-bond orbital with pieces of the surface in the vacancy and other neighboring sites. H atoms are colored black.

Since the wave functions associated with the gap states in the unrelaxed CLOSE and FAR models do not have a single center, but are peaked at the two dangling bonds, we will not analyze the localization by means of the spread in these cases. However, as we show in IIIB.2, relaxation leads in

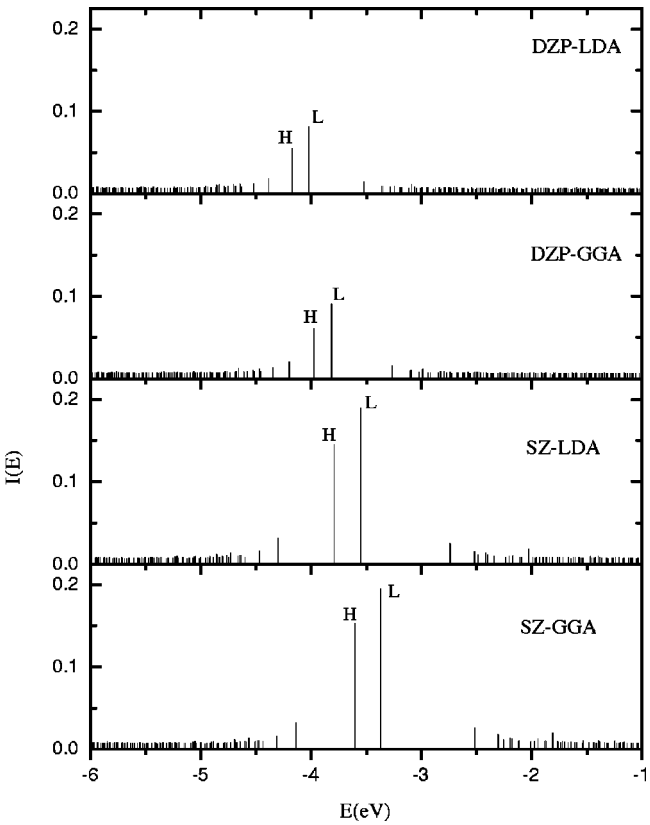

FIG. 4. IPR for the model CLOSE using frozen coordinates. The two highly localized midgap states sit on the central atoms of the two dangling bonds. The state labeled H is the highest occupied molecular orbital (HOMO) and the state labeled L is the lowest unoccupied molecular orbital (LUMO).

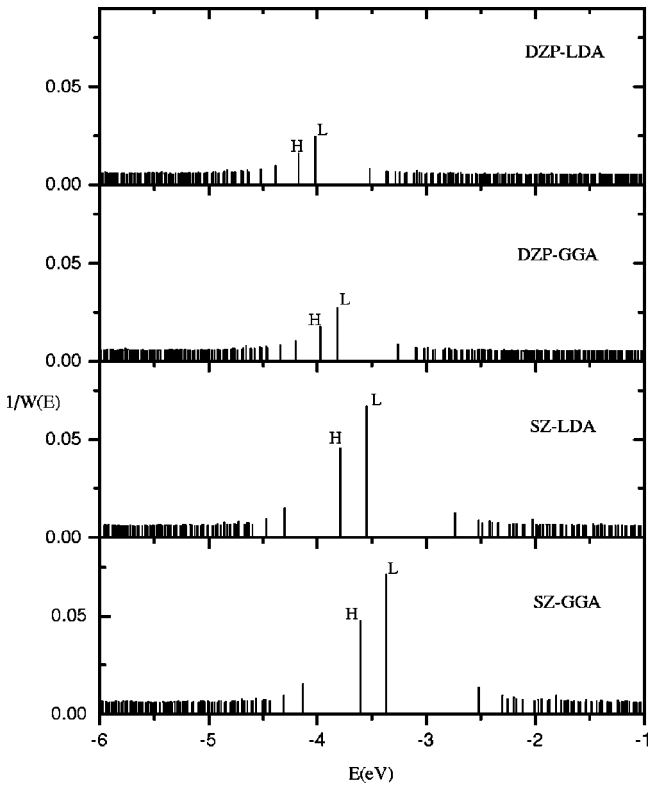

FIG. 5. $1/W(E)$ for the model CLOSE with the atoms frozen.

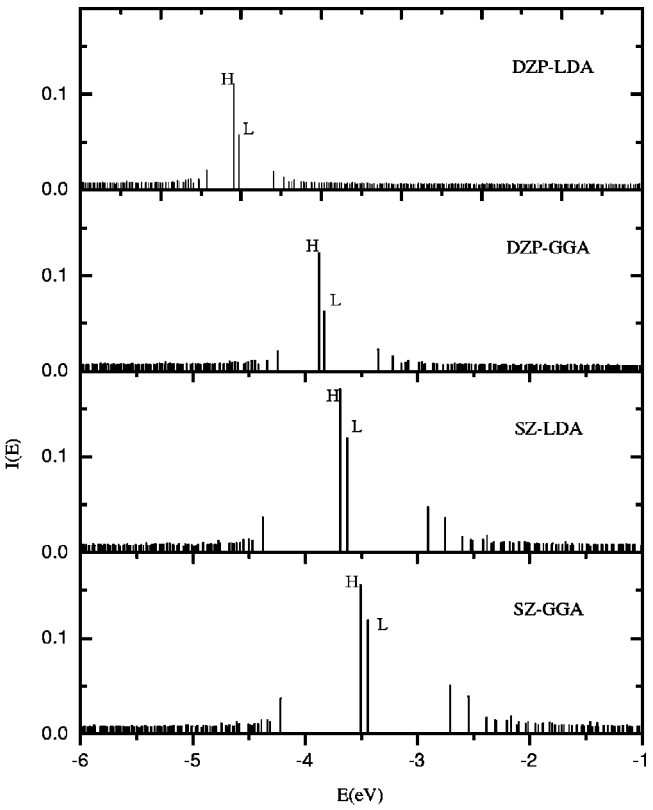

FIG. 6. IPR for the model FAR using frozen coordinates. The two highly localized midgap states (H for HOMO and L for LUMO) are nearly degenerate.

some cases to localization of the wave functions around one of the dangling-bonds, and this will allow us to use the spread in such cases to quantify localization.

Our frozen lattice calculations consistently show that increasing the basis set decreases the localization. Although this is not unexpected, the huge decrease in the localization of the wave function as the size of the basis functions increases from SZ to DZP is quite surprising. The fact that the results are consistent in both the amorphous and crystalline system makes it even more interesting and general. A plausible explanation for this effect is that the energy gap is clearly reduced as the basis set is more complete. The localized states are then closer to the band edges, and therefore are more able to mix with the extended bulk states, becoming more delocalized. Obviously, the delocalization will not proceed indefinitely upon improvement of the basis set, but will converge as the basis approaches completeness.

2. Spin localization versus wave-function localization

Fedders and co-workers[12] have shown that, in order to correlate the degree of localization from dangling-bond states with ESR experiments, it is not enough to look at the wave functions, but to the net spin polarization near the dangling bond. The reason is that the spin density has also contributions from electronic states other than the localized defect wave function, which contribute to make the spin polarization more localized than the specific localized state wave function. In order to confirm this result (obtained by Fedders *et al*. on cells of *a*-Si:H) in our structural models, we performed calculations allowing for spin polarization in our frozen lattice models, using the DZP basis set. Except for the *c*-Si:H case, where there is one unpair electron that yields a net spin polarization, we were not able to find a spin-polarized solution for any of the amorphous cells. The reason is the existence of two interacting dangling bonds, which favors the formation of a spin singlet with two electrons paired. In order to force the appearance of a spin moment in our models, we introduce an unpaired spin by removing a single electron from the system.

In the model *c*-Si:H, we find a contribution of almost 50% to net spin by the central dangling bond and its neighbors (the central atom alone contributing 38%). However, the Mulliken charge contribution to the wave function of the corresponding localized state from the defect site is only $0.29e$. The hydrogen-terminated dangling-bond sites also contribute about 10% of the net spin. The remainder is somewhat distributed uniformly at the other sites. In CLOSE, about 57% of the net spin polarization was due the one dangling bond and its three neighbors. The other dangling bond contributed only 6% to the net spin with essentially zero contribution coming from the neighbors. In FAR, about 54% of the net spin localization sits on the isolated dangling bond and its nearest neighbors. Our results are in good agreement with the previous LSDA calculations by Fedders *et al*.,[12] and in reasonable agreement with the experiment.[10,11]

Our results confirm that, for a dangling-bond defect state, there is a rather large difference between spin localization and wave-function localization. In particular, the degree of

spin localization is greater than that of the wave-function localization at the dangling-bond site. To our knowledge, no experimental methods exist for measuring the extent of wave-function localization on the dangling-bond orbital as opposed to spin.

B. Relaxation effects

1. Geometry of defect sites, density functionals, and basis sets

In this section we discuss the geometry around the defect sites before and after relaxation. The details of the local geometry are very important in determining the local electronic structure and the strain around the defect site, and here we study the dependence with varying basis and density functional. We relax all the models using a conjugate gradient optimization until the largest atomic force is smaller than 0.04 eV/Å.

Relaxation effects for the simple dangling-bond defect in *c*-Si:H are relatively small. There are no major rearrangements in bonding, but only a relaxation of the surroundings of the vacancy site.

In the unrelaxed CLOSE model, the dangling bonds were originally separated by a distance of 4.6 Å. After SZ basis relaxations, both with LDA and GGA, the defect sites come closer, to a distance of about 2.6 Å, to form a highly strained bond. For the more complete DZP basis set, the two defect sites also approach each other, but they continue being undercoordinated, so the two distinct dangling bonds remain present.

In the case of the FAR model, one of the two well separated dangling bonds forms a strained bond with a neighboring atom after a SZ-LDA relaxation. The dangling bond is therefore terminated, and a floating bond is introduced. The other dangling bond remains present. For the SZ-GGA relaxation, the two dangling bonds still continue to exist, but the one that was terminated in the SZ-LDA case also approaches a neighbor and tries to form a bond. After the DZP relaxations, the dangling bonds still exist both in LDA and GGA.

Our results indicate that SZ basis tends to favor tetrahedral bond formation whereas DZP qualitatively preserves the original structure with the dangling bonds present. Also, the SZ tends to favor the transformation of dangling bonds into floating bonds. The results therefore suggest that the richer DZP basis set is necessary for an accurate description of the geometry of both isolated and clustered dangling bonds in amorphous silicon. The SZ basis is not flexible enough to provide sufficient freedom to describe the different shape of the wave function at the dangling bonds compared to covalent sp^3 bonds (for which the basis is ideally suited). Therefore, it tends to favor the disappearance of the dangling bonds through annihilation with other dangling bonds or formation of floating bonds with other already fourfold-coordinated atoms.

2. Localization, density functionals, and basis sets

We now consider in detail the trends in the localization behavior of the electronic states in the gap after full structural relaxations. We also examine the role the defect site in a relaxed environment plays in the localization of gap states. We study the localization using the IPR for each of the three fully relaxed models within the different approximations.

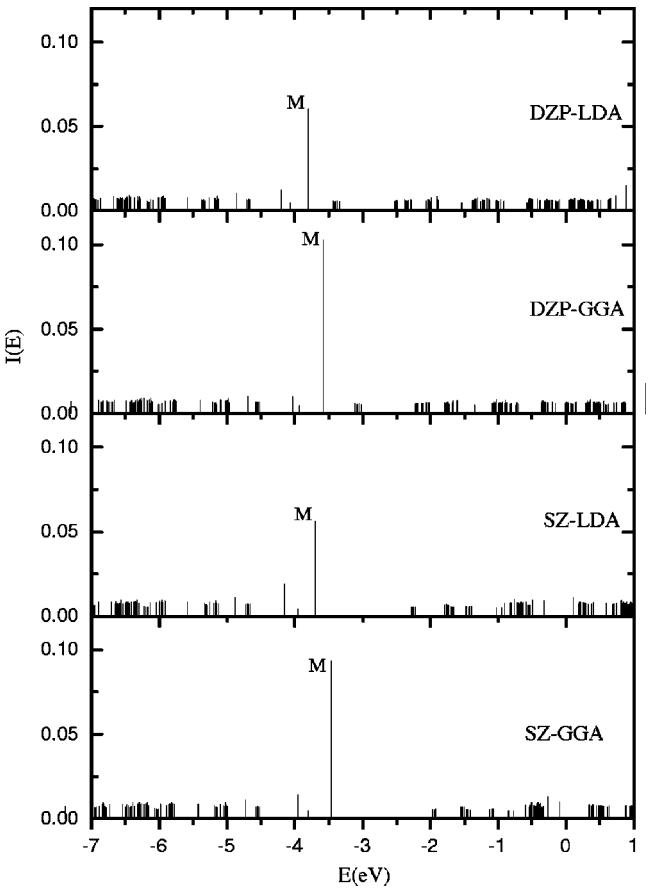

FIG. 7. IPR for the fully relaxed model *c*-Si:H.

We first studied the simple dangling-bond defect in *c*-Si:H. Figure 7 shows that, for the relaxed structures, the localization behavior of the midgap state is density-functional dependent but rather basis-set independent, contrary to the results obtained in the frozen lattice calculations (Fig. 1). In other words, within the same density-functional approximation, SZ yields a similar wave-function localization as DZP for the simple defect in the relaxed crystalline environment. We also see that the GGA defect state is more localized than the LDA defect state for a given basis set. The IPR values obtained with DZP are, nevertheless, almost unchanged upon relaxation, the difference between the unrelaxed and relaxed geometries occurring mainly for the SZ basis. The analysis from the real-space spread, shown in Table II, confirms the results obtained via the IPR. We see again the similarity between SZ and DZP for a given functional, with the GGA states having a smaller spread than LDA.

The IPR for the fully relaxed CLOSE is shown in Fig. 8. As discussed in the preceding section, structural relaxation for this model is basis dependent. We first see that the splitting between the HOMO and LUMO levels is now much larger than in the unrelaxed case. This is attributed to the fact that, in order to minimize the total energy, occupied defect states move down in energy and closer into the valence-band

TABLE II. The spread and integrated charge for the localized midgap state M for the relaxed c-Si:H model.

Functional	Basis	σ^2	q_Ω
LDA	DZP	34.24	0.79
GGA	DZP	27.14	0.84
LDA	SZ	38.42	0.76
GGA	SZ	32.07	0.81

TABLE III. The results for σ^2 and q_Ω corresponding to the localized LUMO state for the relaxed CLOSE model.

Functional	Basis	σ^2	q_Ω
LDA	DZP	31.85	0.76
GGA	DZP	28.14	0.79
LDA	SZ	23.50	0.84
GGA	SZ	22.45	0.87

edge, whereas the unoccupied states do not affect the energy and thus can move towards the conduction-band edge. The second observation is that now the localization of both HOMO and LUMO has decreased considerably compared to the unrelaxed case. Again, this is a consequence of the levels being closer to the band edges, mixing more strongly with the delocalized bulk states and therefore becoming less localized. The effect is larger for the HOMO, which is the one that adjusts its shape to optimize the total energy. A third observation is the appearance of increasingly localized states in the band edges, corresponding to bulk states which start becoming localized and form the precursor of band tails. This effect is originated from the strain field imposed by the relaxation of the sites around the defects. Therefore, the presence of defects such as dangling bonds in amorphous silicon also brings the appearance of band tails of weakly localized states due to the introduction of stress in the surroundings of the defect. This supports results from previous work[38] that there is not a one to one correspondence between spectral and geometric defects. The localization of the tail states decays as one moves deeper into the conduction and valence regions, as was previously observed by Dong and Drabold[39] using a simple orthogonal tight-binding Hamiltonian on a much larger 4096-atom model of a-Si.

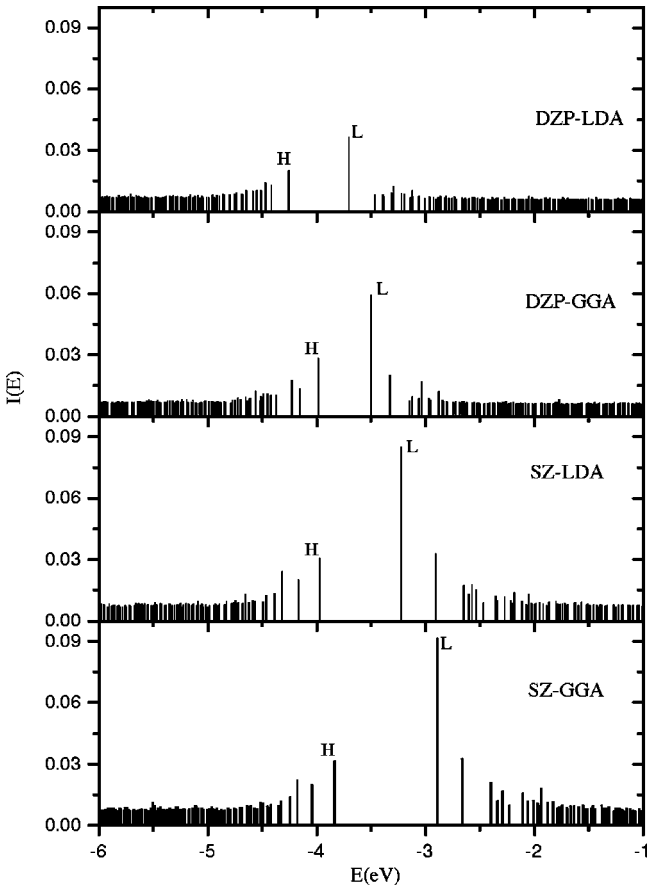

FIG. 8. IPR for the fully relaxed model CLOSE.

We now focus on the evolution of localization with basis set and density functional for the relaxed CLOSE model. As we observed with the c-Si:H case, the HOMO level becomes less localized upon relaxation, especially in the case of the SZ basis, for which the IPR is reduced by more than a factor

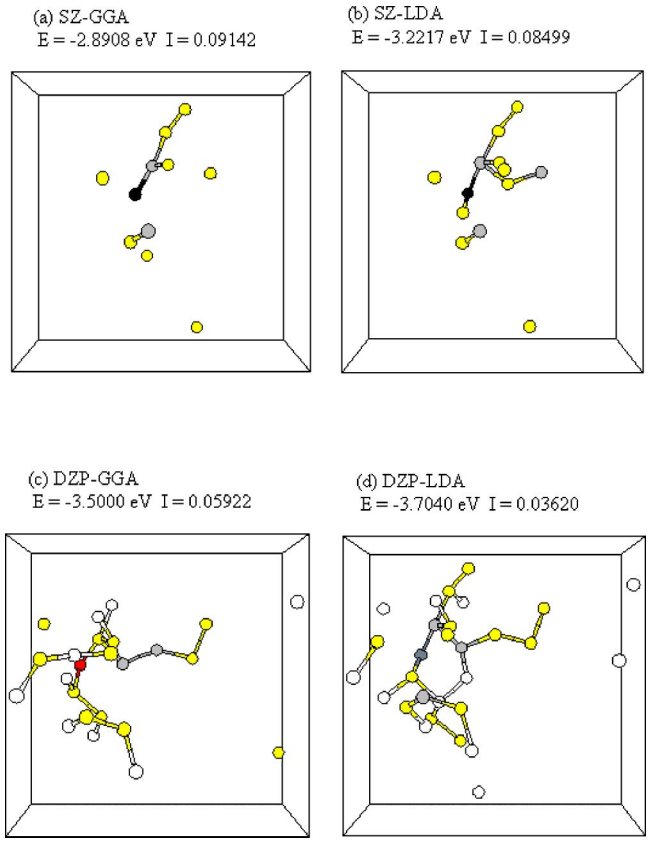

FIG. 9. (Color online) Spatial character of localized eigenstates for the LUMO state for the relaxed CLOSE model. The energy and its corresponding IPR localization are indicated in each picture. We use the following color code to depict the fraction of the Mulliken charge q for the localized state at each atomic site: black ($q>0.25$), red ($0.15<q<0.25$), slate gray ($0.10<q<0.15$), gray ($0.05<q<0.10$), yellow ($0.01<q<0.05$), and white ($q<0.01$). Only 65% of the total charge is shown.

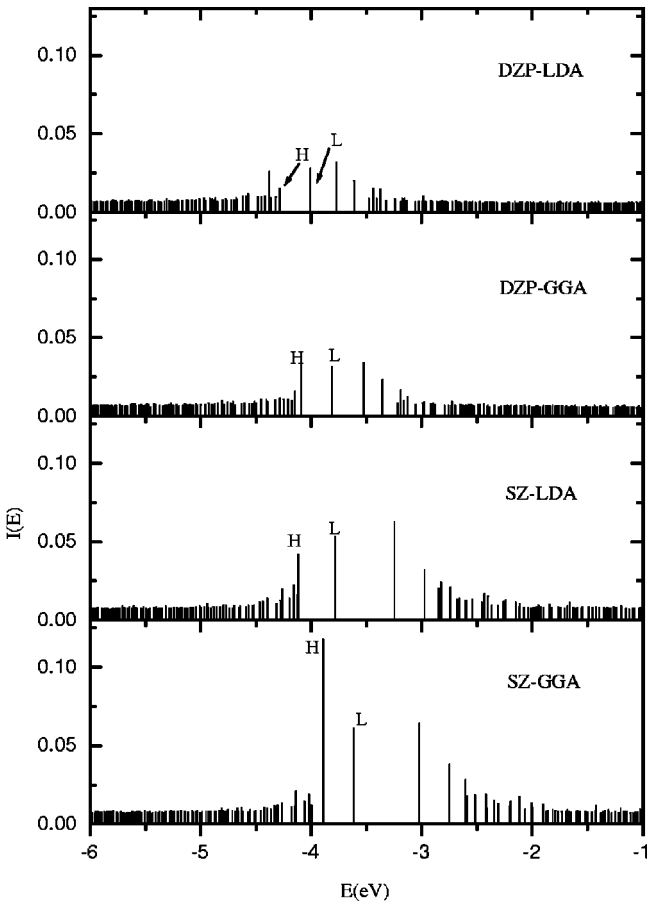

FIG. 10. IPR for the fully relaxed model FAR.

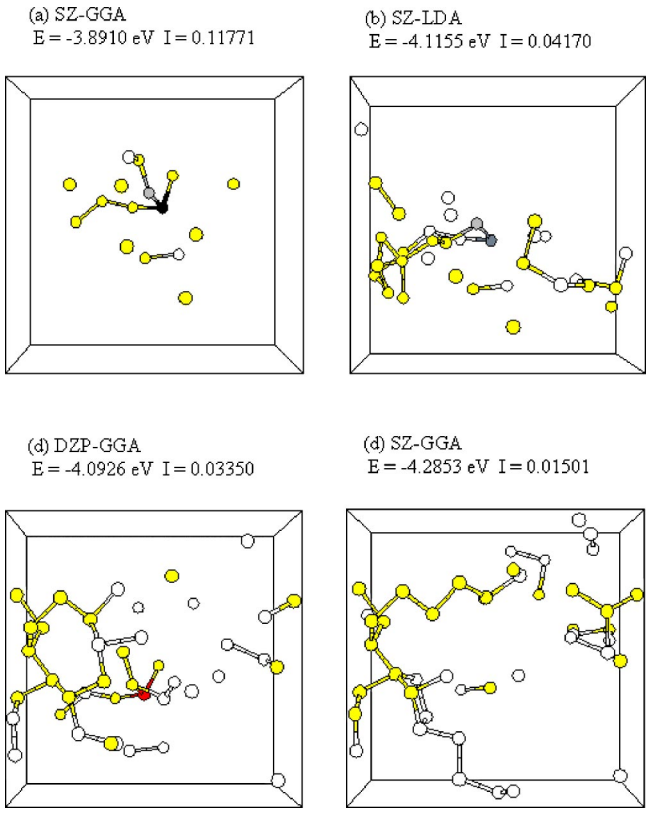

FIG. 11. (Color online) Spatial character of localized eigenstates for the HOMO state for the relaxed FAR model. The color coding is the same as the CLOSE case in Fig. 9.

of 2. The degree of HOMO localization predicted by the SZ and DZP bases for the relaxed structure is therefore very similar. For the LUMO, the difference between SZ and DZP is still large, as in the unrelaxed case. The high IPR values associated with the LUMO in the SZ cases are primarily due to strain (as a result of the bond between the two neighboring dangling-bond atoms). The spread of the LUMO is reported in Table III. We again observe the common trends in the spread: GGA states show slightly less spread compared to LDA, and SZ basis set yields more localized states than DZP basis set.

In order to get a pictorial representation of the localized states in this relaxed model and the evolution with basis set and density functional, we assign different colors to each site according to its Mulliken charge contribution to the given eigenstate. We depict this spatial feature by showing only 65% of the total charge for the LUMO in Fig. 9. We observe a small network connection of atoms for the localized states in Figs. 9(a) and 9(b) but the connectivity spreads out in a rather one-dimensional (1D) fashion, mimicking a chain in Figs. 9(c) and 9(d). The small size of our cell does not allow us to immediately visualize a localized region containing completely the cluster of atoms, which can be done in larger supercell containing thousands of atoms.[39]

We now turn to the relaxed FAR model. In Fig. 10, we have plotted the IPR for the this model, for different density functionals and basis sets. Again, we see the same general features that we pointed out in the relaxed CLOSE case. First, the splitting between HOMO and LUMO is much larger than in the unrelaxed case. Both states, and specially the HOMO, become more delocalized upon relaxation, with the notable exception of the SZ-GGA case, which yields a strongly localized HOMO state. We also see the formation of band tail states, and even the presence of strongly localized states in the gap above the LUMO, due to strong relaxation induced strain fields. Again, in this model, we observe that localization is stronger for GGA than with LDA, and that the difference in localization between SZ and DZP bases is much reduced upon relaxation. The difference in localization for the SZ-GGA and SZ-LDA cases can be explained by the fact that, as mentioned previously, SZ-LDA relaxation results in the disappearance of a dangling-bond and the formation of a floating bond, which are known to be less localized than dangling bond defects.

Finally, we visualize a chosen state (HOMO in this case) for the relaxed FAR model using a color coding in Fig. 11. The Mulliken charge concentrations on the atoms change from confined clusterlike character (or equivalently short 1D strings) in Fig. 11(a) to long stringlike character of atoms in Fig. 11(d) as one tunes the basis and functional from SZ-GGA through to DZP-LDA . The ''tinker-toy'' character can be attributed to less localized states and it is mainly due to weak quantum-mechanical mixing. This behavior has been observed earlier by Drabold *et al.*[39,40]

IV. CONCLUSION

We have performed a first-principles electronic structure calculation on three Si supercells: two 216-atom supercells of amorphous silicon with two dangling bonds and one 218-atom supercell of hydrogenated crystalline silicon with a void. Depending on the initial distance between the dangling bonds, the two *a*-Si models have been classified as CLOSE and FAR. We examined the nature of localized band tail and gap states within the LDA and GGA using both minimal SZ basis and more complete DZP basis with particular attention paid to relaxation effects. Spin localization and wave-function localization for dangling-bond defect states has also been studied. We computed the wave-function localization as the spread of the wave function in real space and via other measures that utilize the Mulliken charges.

For the frozen lattice calculations, we find that the localization of wave functions associated with defect states decreases with larger basis sets and has enhancement of localization using GGA compared to LDA for all the models. The reduction in charges at the atomic sites for a larger basis set can be attributed to the hybridization between the atomic orbitals, providing the electronic charges more degrees of freedom to redistribute themselves. This is reflected in a smaller distance between the defect states and the band-gap edges, which also favors delocalization. Unpaired spin LSDA calculations performed on frozen lattices showed that the degrees of spin and wave-function localization are different. In particular, degree of spin localization at a dangling-bond site is far greater than the degree of wave-function localization. The difference between the localization of a defect state in a fully relaxed and frozen systems is nontrivial, especially in the minimal basis calculations. In particular, there was a considerable reduction in localization (as measured using the Mulliken charge) for the relaxed systems compared to the frozen lattices. We also conclude that a large basis set (DZP in this case) is necessary for an accurate description of both the geometry and localized states associated with defect sites.

ACKNOWLEDGMENTS

We are grateful to Professor Normand Mousseau for sending us his models of amorphous silicon. We also acknowledge the support of the National Science Foundation under Grant Nos. DMR-0074624, DMR-0310933, and DMR-0205858. P.O. acknowledges support for his research visit to Ohio University from the Programa de Movilidad de Investigadores of Ministerio de Educación y Cultura of Spain.

*Electronic address: drabold@helios.phy.ohiou.edu

[1] See, for instance, S.R. Elliot, *Physics of Amorphous Materials* (Longman, London, 1984).
[2] R. Biswas, C.Z. Wang, C.T. Chan, K.M. Ho, and C.M. Soukoulis, Phys. Rev. Lett. **63**, 1491 (1989).
[3] D.C. Allan and E.J. Melle, Phys. Rev. B **31**, 5565 (1985).
[4] P.A. Fedders and A.E. Carlsson, Phys. Rev. B **39**, 1134 (1989).
[5] J. Holender and G. Morgan, J. Phys.: Condens. Matter **4**, 4473 (1992).
[6] S. Kneif and W. von Neissen, Phys. Rev. B **58**, 4459 (1998).
[7] B.J. Min, Y.H. Lee, C.Z. Wang, C.T. Chan, and K.M. Ho, Phys. Rev. B **45**, 6839 (1992).
[8] W. Kohn and L.J. Sham, Phys. Rev. **140**, A1133 (1965).
[9] P.A. Fedders and D.A. Drabold, Phys. Rev. B **47**, 13 277 (1993).
[10] D.K. Biegelsen and M. Stutzmann, Phys. Rev. B **33**, 3006 (1986).
[11] T. Umeda, S. Yamasaki, J. Isoya, and K. Tanaka, Phys. Rev. B **59**, 4849 (1999).
[12] P.A. Fedders, D.A. Drabold, P. Ordejon, G. Fabricius, D. Sanchez-Portal, E. Artcho, and J.M. Soler, Phys. Rev. B **60**, 10 594 (1999).
[13] P. Hohenberg and W. Kohn, Phys. Rev. **136**, B864 (1965).
[14] M.S. Hybertsen and S.G. Louie, Phys. Rev. B **34**, 5390 (1986).
[15] B.G. Pfrommer and S.G. Louie, Phys. Rev. B **58**, 12 680 (1998).
[16] J.-L. Li, G.-M. Rignanese, E.K. Chang, X. Blase, and S.G. Louie, Phys. Rev. B **66**, 035102 (2002).
[17] G.T. Barkema and N. Mousseau, Phys. Rev. B **62**, 4985 (2000).
[18] F. Wooten, K. Winer, and D. Weaire, Phys. Rev. Lett. **54**, 1392 (1985).
[19] P. Ordejón, E. Artacho, and J.M. Soler, Phys. Rev. B **53**, 10441 (1996).
[20] D. Sánchez-Portal, P. Ordejón, E. Artacho, and J.M. Soler, Int. J. Quantum Chem. **65**, 453 (1997)
[21] J.M. Soler, E. Artacho, J.D. Gale, A. García, J. Junquera, P. Ordejón, and D. Sanchez-Portal, J. Phys.: Condens. Matter **14**, 2745 (2002).
[22] J.P. Perdew and A. Zunger, Phys. Rev. B **23**, 5048 (1981).
[23] J.P. Perdew, K. Burke, and M. Ernzerhof, Phys. Rev. Lett. **77**, 3865 (1996).
[24] N. Troullier and J.L. Martins, Phys. Rev. B **43**, 1993 (1991)
[25] L. Kleinman and D.M. Bylander, Phys. Rev. Lett. **48**, 1425 (1982).
[26] O.F. Sankey and D.J. Niklewski, Phys. Rev. B **40**, 3979 (1989).
[27] Single-ζ basis set means one *s* orbital for H valence electron and one *s* and three *p* for Si valence electrons. Double-ζ with polarization orbitals means two *s* and three *d* orbitals for H, and two *s*, six *p*, and five *d* for Si. For details on the generation of the basis orbitals, see E. Artacho, D. Sánchez-Portal, P. Ordejón, A. García, and J.M. Soler, Phys. Status Solidi B **215**, 809 (1999).
[28] A. Szabo and N.S. Ostlund, *Modern Quantum Chemistry* (McGraw-Hill, New York, 1989), p. 151.
[29] J.P. Lewis, J. Pikus, TH.E. Cheatham, E.B. Starikov, Hao Wang, J. Tomfor, and O.F. Sankey, Phys. Status Solidi B **233**, 90 (2002).
[30] J.P. Lewis, J. Pikus, TH.E. Cheatham, E.B. Starikov, Hao Wang, J. Tomfor, and O.F. Sankey, J. Phys. Chem. B **107**, 11 (2003).
[31] C. Shannon, *The Mathematical Theory of Communication* (University of Illinois Press, Urbana, 1949).
[32] E.T. Jaynes, *Probability Theory: The Logic of Science* (Cambridge University Press, Cambridge, 2003).
[33] The information entropy functional is the only form which consistently represents our state of knowledge in a probability theoretic sense. For a discussion of the $p\,log(p)$ functional versus p^2 (as for the IPR of this paper), see Jaynes (Ref. 32), and references therein.

[34] S.F. Boys, in *Quantum Theory of Atoms, Molecules and the Solid State*, edited by P.-O. Löwdin (Academic Press, New York, 1966), p. 253.

[35] N. Mazari and D. Vanderbilt, Phys. Rev. B **56**, 12 847 (1997).

[36] P.L. Silvestrelli, N. Marzari, D. Vanderbilt, and M. Parrinello, Solid State Commun. **107**, 7 (1998); U. Stephan and D.A. Drabold, Phys. Rev. B **57**, 6391 (1998); U. Stephan, R.M. Martin, and D.A. Drabold, *ibid*. **62**, 6885 (2000).

[37] As a preliminary, we note the following dependence of the gap on basis set and density functional. In the LDA, we find gaps of 1.68 eV, 1.35 eV, 0.81 eV, and 0.62 eV, with GGA the sequence reads 1.83 eV, 1.50 eV, 0.94 eV, and 0.82 eV. The order of the numbers is single zeta (SZ), double zeta (DZ), single zeta with polarization orbitals (SZP), and double zeta with polarization orbitals (DZP). Of course these numerical values depend upon the algorithm used to generate the second zeta.

[38] D.A. Drabold, P.A. Fedders, S. Klemm, and O.F. Sankey, Phys. Rev. Lett. **67**, 2179 (1991).

[39] J. Dong and D.A. Drabold, Phys. Rev. Lett. **80**, 1928 (1998).

[40] P.A. Fedders, D.A. Drabold, and S. Nakhmanson, Phys. Rev. B **58**, 15 624 (1998).